

C: Plasmonics; Optical, Magnetic, and Hybrid Materials

**Impact of Bis(imino)pyridine Ligands on
Mesoscale Properties of CdSe/ZnS Quantum Dots**

Mark D Bartolo, Ryan P Brisbin, James C. Fettinger, Sayantani Ghosh, and Ryan D. Baxter

J. Phys. Chem. C, **Just Accepted Manuscript** • DOI: 10.1021/acs.jpcc.0c06335 • Publication Date (Web): 21 Sep 2020Downloaded from pubs.acs.org on September 28, 2020**Just Accepted**

“Just Accepted” manuscripts have been peer-reviewed and accepted for publication. They are posted online prior to technical editing, formatting for publication and author proofing. The American Chemical Society provides “Just Accepted” as a service to the research community to expedite the dissemination of scientific material as soon as possible after acceptance. “Just Accepted” manuscripts appear in full in PDF format accompanied by an HTML abstract. “Just Accepted” manuscripts have been fully peer reviewed, but should not be considered the official version of record. They are citable by the Digital Object Identifier (DOI®). “Just Accepted” is an optional service offered to authors. Therefore, the “Just Accepted” Web site may not include all articles that will be published in the journal. After a manuscript is technically edited and formatted, it will be removed from the “Just Accepted” Web site and published as an ASAP article. Note that technical editing may introduce minor changes to the manuscript text and/or graphics which could affect content, and all legal disclaimers and ethical guidelines that apply to the journal pertain. ACS cannot be held responsible for errors or consequences arising from the use of information contained in these “Just Accepted” manuscripts.

Impact of Bis(imino)pyridine Ligands on Mesoscale Properties of CdSe/ZnS Quantum Dots

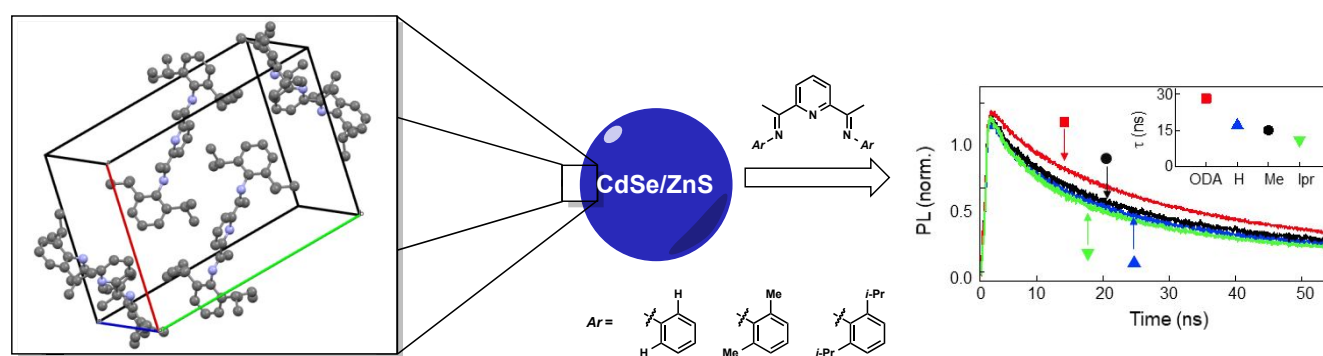
Mark D. Bartolo,^{1‡} Ryan P. Brisbin,^{2‡} James C. Fettingner,³ Sayantani Ghosh,¹ and Ryan D. Baxter^{2*}

¹Department of Physics, School of Natural Sciences, University of California, Merced, CA 95344, USA

²Department of Chemistry and Chemical Biology, School of Natural Sciences, University of California, Merced, CA 95344, USA

³Department of Chemistry, X-Ray Crystallography Laboratory, University of California, Davis, CA 95616

Supporting Information Placeholder



TOC Graphic

ABSTRACT: We investigate the effect of surface modification of CdSe/ZnS quantum dots (QDs) with bis(imino)pyridine (BIP) ligands. BIPs are a class of redox non-innocent ligands known to facilitate charge transfer in base metals on the molecular scale, but their behavior in nano- to meso-scale systems has been largely unexplored. Using electron microscopy, crystallography and ultrafast spectroscopy, we reveal that structure specific π - π stacking of the BIP molecules alters inter-dot separation in QD films, thereby leading to changes in optical and electronic properties. The three variations used are unsubstituted (BIP-H), dimethyl (BIP-Me) and diisopropyl (BIP-Ipr) bis(imino)pyridine, and when compared with the native octadecylamine (ODA) ligand, we find that both energy and charge transfer efficiencies between QDs are increased post-ligand exchange, the highest achieved through BIP-Ipr, despite its larger unit cell volume. We further investigate charge transfer from QD films to conducting (indium tin oxide, ITO) and semiconducting (zinc oxide, ZnO) substrates using time-resolved spectroscopy, and determine that the influence of the ligands is QD band gap dependent. In QDs with large band gap (2.3 eV) the BIP ligands facilitate charge transfer to both ITO and ZnO substrates, but in dots with small band gap (1.9 eV) they pose a hindrance when ZnO is used, resulting in reduced recombination rates. These results highlight the importance of investigating multiple avenues in order to optimize surface modification of QDs based on the end goal. Finally, we verify that BIP ligands hasten the rate of QD photo brightening under continuous illumination, allowing the ensemble to achieve stable emission faster than in their native configuration. Our study sets the stage for novel charge transfer systems in the meso and nanoscale, yielding a diverse selection of new surface ligands for applications such as conductive materials and energy production/storage devices employing QDs.

KEYWORDS: Quantum dots, bis(imino)pyridine, charge transfer, time-resolved spectroscopy, surface functionalization

INTRODUCTION

Semiconducting quantum dots (QDs) are widely implemented in a variety of applications that leverage their size-tunable optical and electronic properties¹⁻³. These include opto-electronic devices, such as, photodetectors⁴⁻⁶, light-emitting diodes⁷, and photovoltaics⁸ among others, as well as devices for biomedical sensing^{9,10} and diagnostics^{11,12}. In order to optimize performance in these platforms, the treatment of QD surfaces is of critical importance, given the dots' large surface-to-volume ratios, and the one effective approach to

surface passivation is *via* the use of organic ligands¹³⁻¹⁵. The most common among these are long chain aliphatic hydrocarbons, which have proven very successful in passivating surface defect-related trap states, thereby suppressing non-radiative recombination and stabilizing the QD core from photo-induced degradation, such as photo-darkening and photo-oxidation¹⁶⁻¹⁹. However, as they insulating molecules they hinder transport of charge carriers within QD films, reducing the conductivity, and consequently,

the performance in opto-electronic applications. Aromatic hydrocarbon molecules have facilitated inter-dot charge transport in QD films when used for surface functionalization owing to the presence of delocalized electrons, but these have occasionally altered the bandgap by reducing the excitonic confinement, especially when used in conjunction with metal complexes^{20–23}. But heterogenous charge transfer is a subject that garners interest not only in QD-based systems but across the scientific spectrum, from photovoltaics to electrodes systems in batteries.²⁴ A specific type of charge transfer using organic ligands being heavily explored is for the purpose of

advancing base metal catalysis and lowering the dependency on noble metals (palladium, rhodium, etc). That area is dominated by a class of organic molecules referred to as “redox non-innocent ligands” (RNI). These ligands have the capability to perform reversible charge transfers between a chelated metal and itself. This ability to participate in charge transfer allows metals like iron and cobalt to perform like rhodium and palladium, respectively, in catalytic reactions, through the process of acting as electron reservoirs.^{25,26} This principle of RNI molecules acting as electron

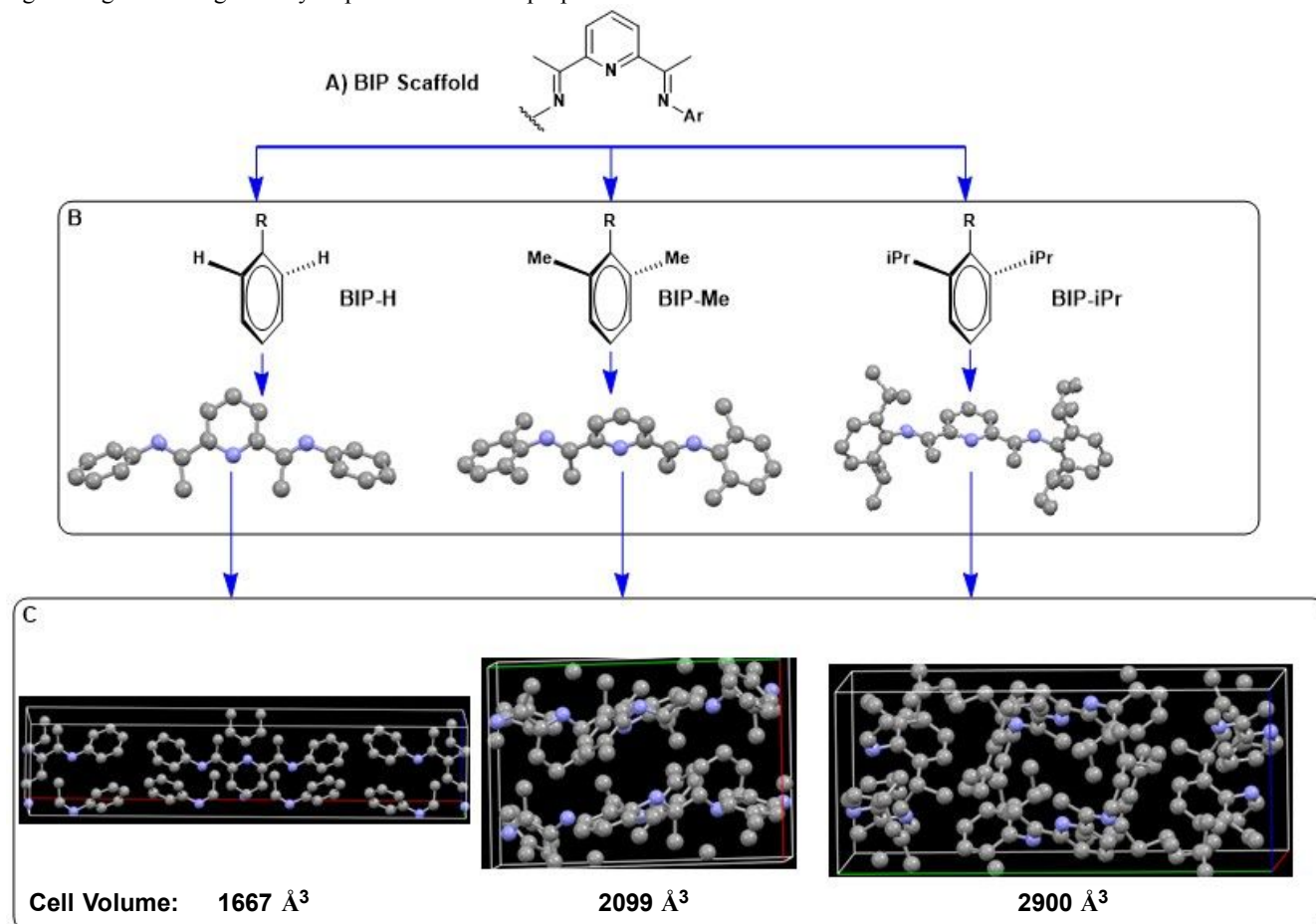


Figure 1. (A) The basic BIP scaffold (B) The three modular units used to design the ligands: BIP-H (unsubstituted BIP), BIP-Me (Dimethyl BIP), and BIP-Ipr (Diisopropyl BIP) (C) Unit cell structures formed by the ligands on crystallization.

reservoirs is highly intriguing and has yet to be applied on systems outside of the molecular scale. In this paper we demonstrate that RNI ligands can be utilized to modulate the opto-electronic properties of non-molecular scale systems such as semiconducting QDs through enhanced inter-dot charge and energy transfer.

We focus on a highly recognizable and well-behaved class of RNI ligands, the bis(imino)pyridine (BIP) scaffold (Figure 1A). The BIP scaffold is used for traditional organometallic chemistry^{27–29} where they function as single-electron reservoirs to facilitate two-electron processes with base metal catalysts. We use three variations of BIPs, unsubstituted (BIP-H), dimethyl (BIP-Me) and diisopropyl (BIP-Ipr) bis(imino)pyridine (Figure 1B) to displace the native ligand, octadecylamine (ODA), of CdSe/ZnS core/shell QDs. Single crystals of each BIP are obtained to provide insights into how these ligands may orient/pack on

the surface of the QDs. Then, using electron microscopy and ultrafast spectroscopy, we reveal that structure specific π - π stacking of the BIP ligands alters inter-dot separation in QD films, which correlates to crystal lattice features of BIPs in the solid state (Figure 1C, unit cells of single-crystal data shown). This change in inter-dot separation leads to remarkable changes in both optical and electronic properties of the BIP-QD film in comparison to the native ligand. These include increases of both energy and charge transfer efficiencies between QDs post-ligand exchange, the highest achieved with BIP-Ipr. We further investigate charge transfer from QD films to conducting (indium tin oxide, ITO) and semiconducting (zinc oxide, ZnO) substrates using time-resolved spectroscopy and determine that the influence of the BIP ligands is QD bandgap dependent. In QDs with large band gap (2.3 eV) the BIP ligands facilitate charge transfer to both ITO and ZnO substrates, but in dots with small band

gap (1.9 eV) they pose a hindrance when ZnO is used, resulting in reduced recombination rates. Surface states also play a significant role in the photo-stability of colloidal QDs^{30,31}. Photo-induced changes include photo brightening, photo darkening and photo-oxidation, all of which result in changes in spectral emission intensity and wavelength over time. These shorten the shelf-life of QD samples and affect performance. The presence of ligands passivates the surface states and arrest these processes to varying degrees^{18,32,33}, and therefore, it is important to investigate this aspect following a ligand exchange. We verify that BIP ligands hasten the rate of QD photo brightening under continuous illumination, allowing the ensemble to achieve stable emission faster than in their native configuration.

RESULTS AND DISCUSSION

To investigate intermolecular packing and size properties of QDs bound with organic BIP ligands, single crystal x-ray analyses were performed on each un-bound ligand shown in **Figure 1**. Substitution at the 2- and 6-position of the aniline sub-units produced solid-state molecular geometries that minimize steric interaction between the aniline and central pyridine units, causing an out of plane tilt of aromatic rings that increases with substituent size (molecular geometries shown in **1B**, *i*-Pr > CH₃ > H for degree of out of plane aromatic tilt). These results are consistent with previous reports of BIP ligands when chelated to a central metal in a Lewis basic fashion.³⁴ Although the geometric configuration of a single BIP ligand may be unsurprising, analysis of unit-cell packing is likely more informative for considering the bulk properties of numerous ligands creating a surface layer on the exterior of QDs. Due to the size disparity between QDs and BIP ligands, direct binding of the central pyridine to the QD surface is unlikely. Alternatively, induced dipole interactions between BIP π -systems and the QD surface could provide electrostatic attraction to promote an alternative mode of binding. Subsequent layers of BIP ligands extending from the QD surface would depend on intermolecular forces between BIP ligands to determine the overall size of the BIP-ligated QDs.

As shown in **Figure 1C**, the unsubstituted BIP-H ligand interacts primarily through the pre-existing dipole of the central pyridine unit, resulting in a tightly packed unit cell with the smallest observed volume and less than 3-angstroms between repeating pyridine units. The reduced steric size of BIP-H renders it the only ligand studied that packed in this fashion. Unit cells for the remaining ligands showed primarily π - π interactions between aniline subunits on neighboring ligand molecules, resulting in larger values for distance of inter-ligand spacing and overall unit cell volume for BIP-Me (3.7 Å spacing, 2099 Å³ volume) and BIP-Ipr (4.5 Å spacing and 2900 Å³ volume) ligands. Such difference in packing and inter-ligand distance affects the physical and electronic properties of QDs ligated with the different BIP ligands, resulting in unique structure-activity relationships for the QDs depending on their environment (*vide infra*).

We summarize the basic spectroscopic characterization of QDs post ligand-exchange in **Figure 2**, along with results of the ODA-ligated control dots for comparison. This is an important check because surface functionalization can cause changes in quantum confinement, which result in an emission red-shift, or proliferation of surface defects, which

may accelerate core photo-oxidation and darkening. Photoluminescence (PL) of CZ640 and CZ500 nm QDs dispersed in solution shown in **Figure 2A** and **2B** confirm that there are no significant changes to any aspect of the emission spectra after the ODA ligands are exchanged by the three variations of BIP. Photoluminescent quantum yield (PLQY) is another critical parameter that directly reflects the impact of ligand exchange. Our measurements do not reveal a significant difference in PLQY between the different QD populations. For ODA, H, Me and IPr the measured PLQYs are 35%, 30%, 36% and 32%, respectively. Time-resolved PL measurements of the QDs in a dilute solution further reveal no distinction between dots functionalized with ODA, BIP-H, BIP-Me and BIP-Ipr, with the recombination time for all four populations being 40 ± 3 ns. **Figure 2C** plots the time-resolved PL curves for QD films deposited on a glass substrate, and the charge recombination lifetimes are calculated by first using a bi-exponential fit $I_{PL} = A_1e^{-t/\tau_1} + A_2e^{-t/\tau_2}$ and then using the results to extract the average lifetime $\tau = (A_1\tau_1^2 + A_2\tau_2^2)/(A_1\tau_1 + A_2\tau_2)$. These values are plotted in the inset and show a clear variation between the native ODA and the BIP ligands, where τ decreases from 30 ns for ODA-QDs to 11 ns for BIP-Ipr. Faster lifetimes are the norm when comparing QDs in films versus isolated QDs in dilute solutions, as inter-dot interactions allow additional routes of charge recombination. These mechanisms, the resultant timescales and associated effects are strongly dependent on surface states and the subsequent modifications, a good overview of which has been previously describe.³⁵⁻³⁷ The most common mechanism is Forster resonant energy transfer (FRET), a dipole-dipole coupling where the efficiency $\varepsilon \sim 1/r^6$, r being the inter-dot separation³⁵. This data would therefore suggest that the distance between QDs in the films, on average, decreases in ODA, BIP-H, BIP-Me and BIP-Ipr functionalized QDs.

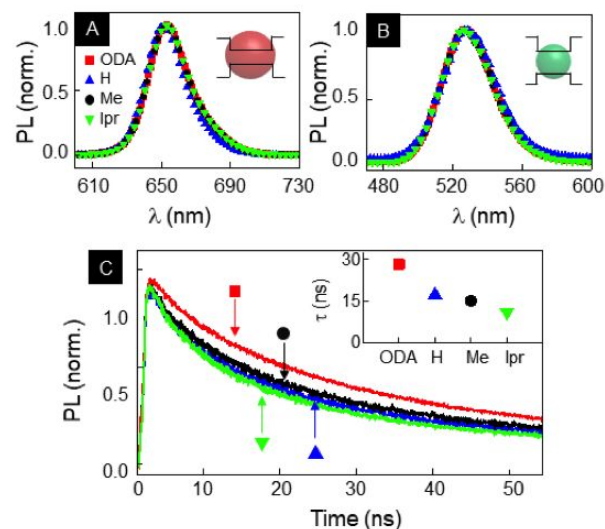


Figure 2. PL emission of (A) CZ640 and (B) CZ500 CdSe/ZnS QDs functionalized with ODA and the three BIP variations. (C) Time-resolved PL for all four populations of QD films deposited on an insulating glass substrate. (Inset) Recombination lifetime τ extracted from exponential fits to the data in the main part.

In an ensemble, FRET occurs as a result of the size inhomogeneity of the QDs, and the roles of donors and acceptors are satisfied by the smaller and larger dots in the population. As a result, the extent of FRET varies with wavelength of the emission spectrum. We verify this in **Figure 3**. Time-resolved PL curves for ODA-QDs with spectral resolution are plotted in **Figure 3A**, and the recombination can be seen to get faster as the emission wavelength at which the data is taken decrease. **Figure 3B** shows the extracted τ across the emission spectrum for all four differently ligated QDs. For ODA-QDs, we notice the expected variation of τ with wavelength, as well as the fact that at the long wavelength end τ approaches the lifetime measured in solution. For the BIP-functionalized QDs the trend is the same, but the shorter lifetimes even at the reddest end of the spectrum imply that the recombination is much faster than the solution values. This would indicate that there is some other route in addition to FRET, and the nature of aromatic ligands would suggest that to be charge transfer.

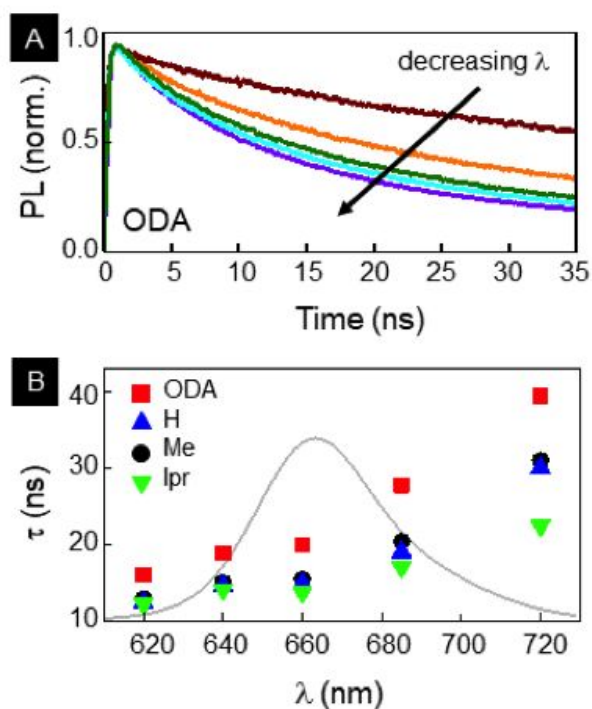


Figure 3. (A) Time-resolved PL curves at different spectral bands of the emission curve for ODA functionalized QD film. Lifetimes decrease with decreasing emission wavelength. (B) Spectrally-resolved recombination times τ for all four QD films superposed on the corresponding spectral region over which they are evaluated.

There remains the possibility that some of the difference in recombination between the ODA-QDs and the BIP-QDs may be due to differences in inter-dot separation. To investigate that, we analyze transmission electron microscopy (TEM) images of close-packed QD films, such as those shown in **Figure 4A** and **4B**, for ODA and BIP-H functionalized QDs, respectively. For each type of QD, we generate a pair-distribution function (PDF) of its TEM image, as shown in **Figure 4C**, which plots the probability of finding a QD at a separation r from another QD. The first peak of this PDF is the average nearest-neighbor distance between the dots, and from this main figure which shows the

PDF of ODA functionalized QDs, that distance is 8.3 nm. Similar analyses of the other QDs return varying QD separations and are plotted in the inset as a function of volume of the ligand unit cells. The inverse relation provides an interesting insight into the packing efficiency of the different ways the three BIP ligands stack. But it also implies there is a variation in FRET efficiency based on the ligand on the QDs. As shown in **Figure 1C**, the shape of the packing units (unit cells) is not uniform across the three BIPs studied. This shape disparity likely affects the mode of ligand stacking on QD surfaces, which should directly impact inter-dot separation.

We return to the averaged lifetimes of the QD films in the inset of **Figure 2C** and using τ of ODA-QDs in film and solution, calculate an efficiency $\epsilon_{Total} = 1 - \tau_{film}/\tau_{solution}$ ³⁹. As ODA is insulating, it is reasonable that energy transfer is the only inter-dot interaction among these QDs, and given that, we extract the FRET constant R_o using $\epsilon_{Total} = \epsilon_{FRET} = 1 / (1 + (r/R_o)^6)$. R_o is defined as the separation where $\epsilon_{FRET} = 50\%$ and is theoretically calculated using the overlap integral of the donor emission spectrum with the acceptor absorption spectrum and their mutual molecular orientation. Here, we evaluate it by equating the two expressions of ϵ_{FRET} and estimate $R_o = 7$ nm, which is very close to the rigorously calculated value of ~ 6.8 nm. Then, we calculate ϵ_{FRET} for the QDs ligated with the BIP ligands using this distance dependent relation and the same R_o and when plotted in **Figure 4D**, it highlights that FRET does increase in case of the BIP-functionalized QDs. However, when we calculate ϵ_{Total} for the BIP-QDs using the formulation involving recombination times, those values are significantly greater than what is accounted for by FRET. For example, $\epsilon_{Total} = 54\%$ for BIP-H QDs but $\epsilon_{FRET} = 33\%$. We attribute this difference to charge transfer, and calculate that efficiency $\epsilon_{Total} - \epsilon_{FRET} = \eta$ to be 21% (BIP-H), 28% (BIP-Me) and 30% (BIP-Ipr) functionalized QDs. The increase of η between the different BIP ligands follows the trend of ϵ_{FRET} in them, both getting larger as inter-dot separation decreases in the QD films. To identify the nature and mechanism of charge transfer, we note that the BIP ligands are photogenerated hole-acceptors as their highest occupied molecular orbital (HOMO) aligns above the QD valence band. BIPs share similar structural elements with a well-known high efficiency hole acceptor, Triazatruxene (TAT). The similarities between TAT and BIPs is significant with both molecules comprising of primarily SP² hybridized carbons and nitrogens, as well as having extensive π character. This extensive π character is known to facilitate hole mobility and stabilize charged states through a reduction in the energy gap between the HOMO and LUMO bands. Along with extensive π pi character, various hetero atoms (nitrogens) also facilitate charge stabilization.⁴⁰

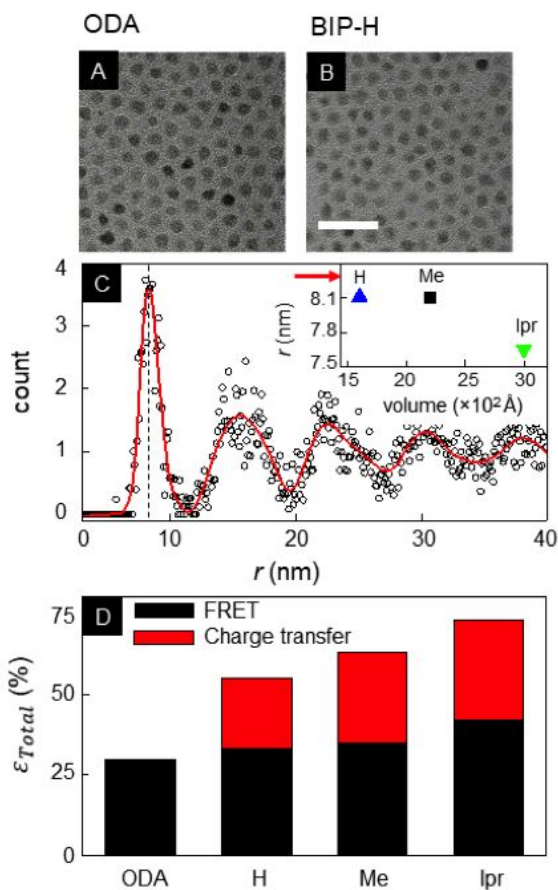


Figure 4. TEM images of drop-cast QD films with (A) ODA and (B) BIP-H ligands. Scale bar: 50 nm. (C) Radial distribution of inter-dot separation r obtained from TEM images and (inset) r values of the BIP variations plotted with unit cell volume. Arrow indicates r for ODA functionalized QDs. (D) Energy and charge transfer efficiencies for the four QD populations.

While inter-QD charge transfer is important or optimal device performance, efficient and fast charge extraction at electrodes or other interfaces is also a necessity. With this in mind, we investigate the recombination dynamics of the QD films when deposited on metallic and semiconducting substrates. The four differently ligated QDs are spin coated onto indium tin oxide (ITO) coated glass and on optically polished n -type zinc oxide (n -ZnO) single crystalline sample. The recombination time τ for both sized QDs on the two substrates are shown in **Figure 5A** and **5B**. For CZ500 (the smaller QDs with the larger bandgap) charge recombination times when ligated with ODA, while expectedly shorter than on glass, are nearly

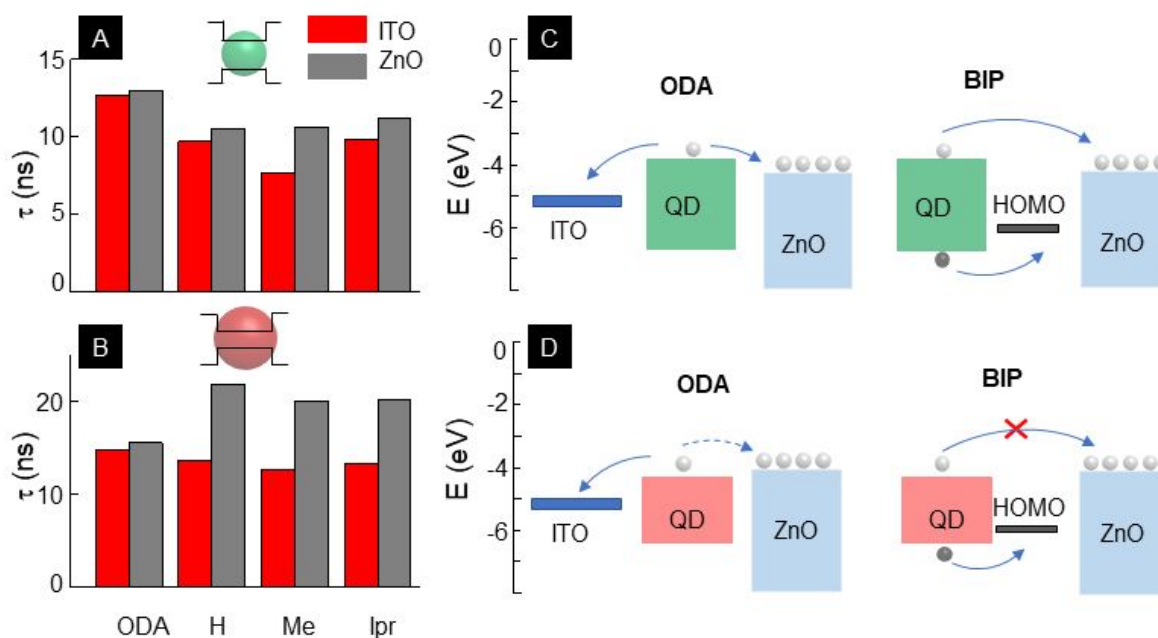


Figure 5. Recombination times τ for (A) CZ500 and (B) CZ640 QD films functionalized with ODA and the BIP ligands, when deposited on conducting indium tin oxide (ITO) and semiconducting n -ZnO substrates. (C, D) Schematics sketching the charge transfer routes for the differently sized QDs.

the same (12.6 and 13 ns) on ITO and ZnO. When functionalized with BIP variations, recombination does get

faster for both substrates, which may be attributed to the charge delocalization of the aromatic rings resulting in a

narrowing of the band gap between the QDs and substrates.⁴¹⁻⁴⁴ The schematics in **Figure 5C** demonstrates the relative band alignments of ITO and ZnO with the QD. The positional advantage of the QD conduction band makes electron transfer to either substrate energetically favorable when functionalized with ODA (**Figure 5C, left**). But the hole-accepting nature of the BIP ligands allows both electrons and holes to be transferred away from the QD core, resulting in the of faster recombination in the BIP-QDs (**Figure 5C, right**)

The same measurements for CZ640 QDs, which are larger and therefore have a smaller bandgap, have different results. For ODA, τ is again very similar on ITO and ZnO (14.7 and 15.3 ns, respectively). As the left schematic in **Figure 5D** shows, electron transfer to ITO is clearly favorable. Although the conduction band of ZnO ~ 0.1 eV above that of the QD, stochastic electron transfer is allowed. BIP-QDs show minor increase in electron transfer to ITO, driven again by the delocalized charges of the ligands. However, the change in recombination rate when BIP-QDs are deposited on ZnO is both significant and unexpected. Recombination lifetimes of BIP-QDs are approximately 30% longer than that of ODA-QDs, indicating that functionalization by the BIP ligands, while facilitating hole transfer, somehow prevents electron transfer from the QD. As the excitation energy used in our studies is smaller than the wide bandgap of ZnO, the presence of oxygen vacancies makes as-grown ZnO highly *n*-doped. Therefore, a possibility is that the delocalized electron cloud of the BIP ligands not only interacts with the photogenerated electrons in the QD core, but also with those in the conduction band of ZnO. This has no consequence for the smaller QDs, where the difference between the energy levels of the QD core and ZnO drives electrons from the former to the latter. The near alignment of conduction bands in the case of the larger QDs and ZnO removes the advantage of this driving potential and concludes with the BIP ligands preventing electron extraction, while still allowing hole transfer. As a result, the recombination rate drops. This modulation of charge carrier transfer based on band alignment between the QDs and the substrates mediated by the BIP ligands is an interesting find, as it opens up the possibility of tailoring functionalization based on specific needs of an application. An important point to note here is that while the charge transfer efficiency η in the QD films is ligand dependent, as shown in **Figure 4D**, in this demonstration of charge transfer from QDs to ITO and ZnO, there is little variation of the same with the different BIP ligands. We attribute this distinction to the fact that while charge transfer in the former is determined by inter-QD separation, for the latter the energetics control the efficiency. A second look at **Figure 4D** shows that η in ascending order is IPr > Me > H, and as the inset in **Figure 4C** confirms, inter-dot separation follows H > Me > IPr. This is also the reason that no charge transfer is observed when the QDs are in solution. Transfer to substrates is nearly independent of which BIP ligand is used as the HOMO levels of all three are within 0.5 eV of each other and are therefore all nearly equivalently aligned with the QD valence band.

But as mentioned earlier, the influence of ligands extends beyond that of transient charge transfer. Modification of QD surfaces may adversely affect long term photo stability of the

QDs, and in **Figure 6** we compare how functionalization with BIP ligands alter photo induced effects. **Figure 6A** plots the spectrally-integrated PL intensity for ODA-QDs over time under continuous photo excitation. It increases rapidly for the first 20 min and then continues to rise at a slower rate. This photo-brightening is a sign that there exist trap states within the bandgap of the core, most likely at the core-shell interface. Photo-generated carriers saturate these states, effectively de-activating non-radiative recombination centers, resulting in increasing PL. But over the same time frame, the FWHM of the QD ensemble increases, which, coupled with a small blue-shift of the emission wavelength, suggests there is photo-oxidation of the QD core. As this reduces the core diameter, the size inhomogeneity of the ensemble is worsened, and the spectral width enhanced. In contrast, the photo-brightening of BIP-H QDs stabilize much faster and there is no observable increase in the emission FWHM over time. It is known that hole-accepting ligands can passivate QD surfaces more effectively than insulating ones⁴¹ and our results confirm that here. It is also an important result as it demonstrates there are no detrimental long-term stability effects as a result of the BIP ligands.

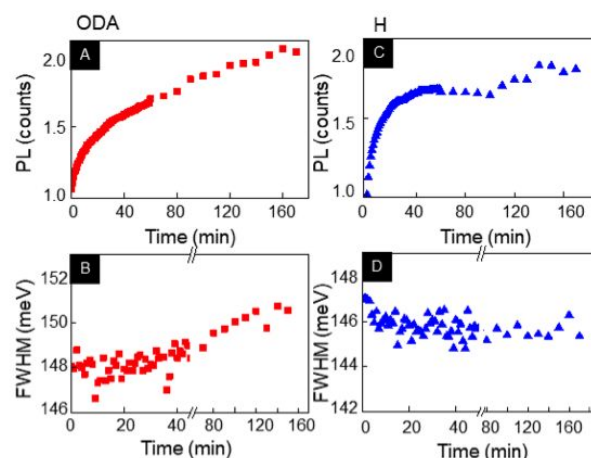


Figure 6. (A) Spectrally-integrated PL intensity and (B) FWHM of emission spectra for ODA-functionalized QDs under constant photoexcitation as functions of illumination time. (C) Spectrally-integrated PL intensity and (B) FWHM of emission spectra for BIP-H-functionalized QDs measured under the same conditions.

CONCLUSIONS

Heterogenous charge transfer has continued to be a critical area of advancement in science due to the increase in demand of society on technology that predicated itself off interfacial charge movement. The role of heterogenous charge transfer in modern conveniences such as smart phones to energy infrastructure *cannot be underrepresented*. This importance on understanding heterogenous charge transfer has set the stage for this work and has shown both a novel and nuanced approach in which to modulate the kinetics of meso-scale heterogenous charge transfer. This was accomplished through the functionalizing semi-conducting quantum dots with redox non-innocent (RNI) ligands as hole acceptors. Through non-standard application of these RNI ligands, *controlled modulation* of the charge transfer dynamics has been achieved on meso-scale material. Moreover, this study has *illuminated* an intriguing band gap dependence on the photoluminescent recombination

lifetimes, which can be observed across both deposited substrates of ITO and ZnO. While interesting, further work is needed in terms of characterizing the complex charge transfer dynamics as well as the effect of other RNI type ligands through tuning of the band gap.

METHODS

Representative Ligand Synthesis: Bis(imino)pyridine ligands were synthesized through azeotropic distillation of 2,6-diacetylpyridine in toluene with the corresponding aniline. 2,6-diacetylpyridine (3 mmols), the aniline derivative (12 mmol), and *p*-toluenesulfonic acid (0.3 mmol) were added to a flame-dried 250ml round bottom flask. Dry toluene (100 ml) was added and the resulting mixture was refluxed using a Dean-Stark apparatus for 24 hours. The reaction mixture was cooled to room temperature and aqueous saturated sodium bicarbonate (100 ml) was added. This mixture was transferred to a separatory funnel the organic layer was extracted. The aqueous layer was washed 3-4 times with dichloromethane and the organic layers were combined, dried with sodium sulfate, and concentrated. The resulting concentrate was dissolved in 15-20 ml of methanol and placed at -20 Celsius for approximately 12 hours. The resulting yellow solid was vacuum filtered and washed with cold methanol. ¹H-NMR was used to assess purity and recrystallization in cold methanol was performed if impurities were detected. Single crystals were grown through solvation in hot methanol and allowed to cool over night at room temperature.

Ligand Exchange: ODA-capped CdSe/ZnS QDs CZ640 (bandgap 1.91 eV) and CZ500 (bandgap 2.3 eV) were purchased from NN-Labs. CZ640 QDs have a core diameter of 4.8 nm (5-10% size inhomogeneity) and CZ500, a 2.0 nm core diameter (10-15% size inhomogeneity). Their surfaces were modified using BIP-H, BIP-Me, and BIP-Ipr. Surface exchange was carried out under inert conditions by adding the QDs to a hexane solution containing an excess of the modifying ligands relative to the native ODA. This solution is incubated for at least 5 minutes and then purified with acetonitrile (MeCN) and chloroform (CHCl₃). The QDs are then separated by centrifugation and dispersed in hexanes for optical measurements.

Sample preparation: For analysis in solution, the QDs were housed in 2.5 mL glass vials. For measurements of QD films, the dots were spin-coated onto glass, ITO (indium tin oxide), and *n*-ZnO (zinc oxide) substrates at 4500 rpm for 15 s, followed by annealing in an oven for 50° C for 30 minutes.

Spectral characterization: For static spectroscopy we use a Princeton Instruments SP2300i spectrometer coupled to a thermo-electrically cooled deep depletion and low noise charge coupled detector, with a spectral resolution of 0.18 nm. An NKT Photonics Super-K laser tuned to 430 nm is used for excitation. For time-resolved measurements, the Super-K is set to a repetition rate of 26 MHz and the collected signal is first dispersed by the spectrometer, and then directed onto a single photon avalanche diode (SPAD) coupled to a PicoHarp 300 time-correlated single photon counting system (TCSPC) with an instrument response function of 28 ps.

Transmission Electron Microscopy (TEM): QD solutions were pipetted onto Pure C on 300 mesh Cu grids and left to

dry overnight in an oven at 50°C, then imaged in Thermo Fisher's Talos F200C G2 TEM.

ASSOCIATED CONTENT

Supporting Information

The Supporting Information is available free of charge on the ACS Publications website.

AUTHOR INFORMATION

Corresponding Author

* rbaxter@ucmerced.edu

Author Contributions

The manuscript was written through contributions of all authors. ‡M.D.B and R.P.B contributed equally to the described work.

ACKNOWLEDGMENT

This material is based upon work supported by the National Science Foundation under Grant Nos. NSF-CAREER 1752821 (R.D.B) and NSF-CREST HRD-1547848 (S. G., M.D.B and R.P.B.)

REFERENCES

1. Moreels, I. *et al.* Size-tunable, bright, and stable PbS quantum dots: A surface chemistry study. *ACS Nano* **5**, 2004–2012 (2011).
2. Wei, G. *et al.* Size-tunable Lateral Confinement in Monolayer Semiconductors. *Sci. Rep.* **7**, 1–8 (2017).
3. Fan, Q. *et al.* Lead-Free Halide Perovskite Nanocrystals: Crystal Structures, Synthesis, Stabilities, and Optical Properties. *Angew. Chemie - Int. Ed.* **59**, 1030–1046 (2020).
4. Grotevent, M. J. *et al.* Nanoprinted Quantum Dot-Graphene Photodetectors. *Adv. Opt. Mater.* **7**, 3–9 (2019).
5. Livache, C. *et al.* A colloidal quantum dot infrared photodetector and its use for intraband detection. *Nat. Commun.* **10**, 1–10 (2019).
6. Sukhovatkin, V., Hinds, S., Brzozowski, L. & Sargent, E. H. Colloidal quantum-dot photodetectors exploiting multiexciton generation. *Science (80-.)*. **324**, 1542–1544 (2009).
7. Yu, S. *et al.* Enhanced optical and thermal performance of white light-emitting diodes with horizontally layered quantum dots phosphor nanocomposites. *Photonics Res.* **6**, 90 (2018).
8. Cho, C., Song, J. H., Kim, C., Jeong, S. & Lee, J. Y. Broadband light trapping strategies for quantum-dot photovoltaic cells (>10%) and their issues with the measurement of photovoltaic characteristics. *Sci. Rep.* **7**, 1–9 (2017).
9. Khan, S. A., Smith, G. T., Seo, F. & Ellerbee, A. K. Label-free and non-contact optical biosensing of glucose with quantum dots. *Biosens. Bioelectron.* **64**, 30–35 (2015).
10. Tajarrud, N., Rofouei, M. K., Masteri-Farahani, M. & Zadmand, R. A quantum dot-based fluorescence sensor for sensitive and enzymeless detection of creatinine. *Anal. Methods* **8**, 5911–5920 (2016).
11. Brazhnik, K. *et al.* Quantum dot-based lab-on-a-bead system for multiplexed detection of free and total prostate-specific antigens in clinical human serum samples. *Nanomedicine Nanotechnology, Biol. Med.* **11**, 1065–1075 (2015).
12. Sukhanova, A. *et al.* Oriented conjugates of single-domain antibodies and quantum dots: Toward a new generation of ultrasensitive diagnostic nanoprobe. *Nanomedicine Nanotechnology, Biol. Med.* **8**, 516–525 (2012).
13. Yang, X. *et al.* Hydroiodic Acid Additive Enhanced the Performance and Stability of PbS-QDs Solar Cells via Suppressing Hydroxyl Ligand. *Nano-Micro Lett.* **12**, 1–12 (2020).

14. Chuang, C. H. M., Brown, P. R., Bulović, V. & Bawendi, M. G. Improved performance and stability in quantum dot solar cells through band alignment engineering. *Nat. Mater.* **13**, 796–801 (2014).
15. Choi, M. J. *et al.* Cascade surface modification of colloidal quantum dot inks enables efficient bulk homojunction photovoltaics. *Nat. Commun.* **11**, 1–9 (2020).
16. Krivenkov, V. *et al.* Ligand-Mediated Photobrightening and Photodarkening of CdSe/ZnS Quantum Dot Ensembles. *J. Phys. Chem. C* **122**, 15761–15771 (2018).
17. Zhang, Y. & Clapp, A. Overview of stabilizing ligands for biocompatible quantum dot nanocrystals. *Sensors* **11**, 11036–11055 (2011).
18. Cao, Y., Stavrinadis, A., Lasanta, T., So, D. & Konstantatos, G. The role of surface passivation for efficient and photostable PbS quantum dot solar cells. *Nat. Energy* **1**, 1–6 (2016).
19. Hines, D. A. & Kamat, P. V. Quantum dot surface chemistry: Ligand effects and electron transfer reactions. *J. Phys. Chem. C* **117**, 14418–14426 (2013).
20. Seker, F., Meeker, K., Kuech, T. F. & Ellis, A. B. Surface chemistry of prototypical bulk II-VI and III-V semiconductors and implications for chemical sensing. *Chem. Rev.* **100**, 2505–2536 (2000).
21. Yoshihara, T., Druzhinin, S. I. & Zachariasse, K. A. Fast intramolecular charge transfer with a planar rigidized electron donor/acceptor molecule. *J. Am. Chem. Soc.* **126**, 8535–8539 (2004).
22. Slama-Schwok, A., Blanchard-Desce, M. & Lehn, J. M. Intramolecular charge transfer in donor-acceptor molecules. *J. Phys. Chem.* **94**, 3894–3902 (1990).
23. Tamai, K. *et al.* Visible-Light Selective Photooxidation of Aromatic Hydrocarbons via Ligand-to-Metal Charge Transfer Transition on Nb₂O₅. *J. Phys. Chem. C* **121**, 22854–22861 (2017).
24. Sevov, C. S. *et al.* Physical Organic Approach to Persistent, Cyclable, Low-Potential Electrolytes for Flow Battery Applications. *J. Am. Chem. Soc.* (2017) doi:10.1021/jacs.7b00147.
25. Chirik, P. J. & Wieghardt, K. Radical ligands confer nobility on base-metal catalysts. *Science* (2010) doi:10.1126/science.1183281.
26. Kaim, W. Manifestations of noninnocent ligand behavior. *Inorganic Chemistry* (2011) doi:10.1021/ic2003832.
27. Small, B. L., Brookhart, M. & Bennett, A. M. A. Highly active iron and cobalt catalysts for the polymerization of ethylene [18]. *Journal of the American Chemical Society* (1998) doi:10.1021/ja9802100.
28. Lyaskovskyy, V. & De Bruin, B. Redox non-innocent ligands: Versatile new tools to control catalytic reactions. *ACS Catalysis* (2012) doi:10.1021/cs200660v.
29. Docherty, J. H., Peng, J., Dominey, A. P. & Thomas, S. P. Activation and discovery of earth-abundant metal catalysts using sodium tert-butoxide. *Nat. Chem.* (2017) doi:10.1038/nchem.2697.
30. Bol, A. A. & Meijerink, A. Luminescence quantum efficiency of nanocrystalline ZnS:Mn²⁺: 2. Enhancement by UV irradiation. *J. Phys. Chem. B* **105**, 10203–10209 (2001).
31. Xu, L., Chen, K., El-Khair, H. M., Li, M. & Huang, X. Enhancement of band-edge luminescence and photo-stability in colloidal CdSe quantum dots by various surface passivation technologies. *Appl. Surf. Sci.* **172**, 84–88 (2001).
32. Yoo, D. *et al.* Origin of the Stability and Transition from Anionic to Cationic Surface Ligand Passivation of All-Inorganic Cesium Lead Halide Perovskite Nanocrystals. *J. Phys. Chem. Lett.* **11**, 652–658 (2020).
33. Frederick, M. T. & Weiss, E. A. Relaxation of exciton confinement in CdSe quantum dots by modification with a conjugated dithiocarbamate ligand. *ACS Nano* **4**, 3195–3200 (2010).
34. Bart, S. C., Lobkovsky, E. & Chirik, P. J. Preparation and molecular and electronic structures of iron(0) dinitrogen and silane complexes and their application to catalytic hydrogenation and hydrosilylation. *J. Am. Chem. Soc.* (2004) doi:10.1021/ja046753t.
35. Zhang, J., Tolentino, J., Smith, R., Zhang, J., Beard, M., Nozik, A. Law, M. Johnson, J. Carrier Transport in PbS and PbSe QD Films Measured by Photoluminescence Quenching. *Journal of Physical Chemistry C*. **118**, 16228–16235. (2014)
36. Zhao, K. Zhong, X. Charge Recombination Control for High Efficiency Quantum Dot Sensitized Solar Cells. *Journal of Physical Chemistry Letters*. **7**, 406–417. (2016)
37. Tagliazucchi, M. Tice, D. Morris-Cohen, A. Weiss, E. Ligand Controlled Rates of Photoinduced Electron Transfer in Hybrid CdSe Nanocrystal/Poly(viologen) Films. *ACS Nano*, **5**, 9907–9917.(2011)
38. Crooker, S. A., Hollingsworth, J. A., Tretiak, S. & Klimov, V. I. Spectrally Resolved Dynamics of Energy Transfer in Quantum-Dot Assemblies: Towards Engineered Energy Flows in Artificial Materials. *Phys. Rev. Lett.* **89**, 186802 (2002).
39. Rodarte, A. Pandolfi, R. Ghosh, S. Hirst, L. Quantum dot/liquid crystal composite materials: self-assembly driven by liquid crystal phase transition templating. *Journal of Materials Chemistry C*. **35**, 5527–5532(2013)
40. Urieta-Mora, J. Garcia-Benito, I, Molina-Ontoria, A. Martín, N. Hole transporting materials for perovskite solar cells: a chemical approach. *Chemical Society Reviews*, **23**, 8541–8571 (2018)
41. Lyaskovskyy, V. & de Bruin, B. Redox Non-Innocent Ligands: Versatile New Tools to Control Catalytic Reactions. *ACS Catal.* **2**, 270–279 (2012).
42. Kaim, W. The shrinking world of innocent ligands: Conventional and non-conventional redox-active ligands. *Eur. J. Inorg. Chem.* **343–348** (2012)
43. Pitchaiya, S. *et al.* A review on the classification of organic/inorganic/carbonaceous hole transporting materials for perovskite solar cell application. *Arab. J. Chem.* **13**, 2526–2557 (2020).
44. Urieta-Mora, J., García-Benito, I., Molina-Ontoria, A. & Martín, N. Hole transporting materials for perovskite solar cells: a chemical approach. *Chem. Soc. Rev.* **47**, 8541–8571 (2018).
45. Tan, Y., Jin, S. & Hamers, R. J. Influence of hole-sequestering ligands on the photostability of CdSe quantum dots. *J. Phys. Chem. C* **117**, 313–320 (2013)..